UC Santa Cruz
UC Santa Cruz Previously Published Works

Title

Dynamics and efficiency of magnetic vortex circulation reversal

Permalink

https://escholarship.org/uc/item/2wt315s2

Journal

Physical Review B, 91(9)

ISSN

2469-9950

Authors

Urbánek, Michal
Uhlíř, Vojtěch
Lambert, Charles-Henri
et al.

Publication Date

2015-03-01

DOI

10.1103/physrevb.91.094415

Peer reviewed

Dynamics and efficiency of the magnetic vortex circulation reversal

M. Urbánek[1,2], V. Uhlíř[1,3], C-H. Lambert[3], J. J. Kan[3], N. Eibagi[3], M. Vaňatka[2], L. Flajšman[2], R. Kalousek[2], M-Y. Im[4], P. Fischer[4], T. Šikola[1,2], E. E. Fullerton[3]

[1]CEITEC BUT, Brno University of Technology, Technická 10, 616 00 Brno, Czech Republic

[2]Institute of Physical Engineering, Brno University of Technology, Technická 2, 616 69 Brno, Czech Republic

[3]Center for Magnetic Recording Research, University of California, San Diego, 92093-0401 La Jolla, California, USA

[4]Center for X-ray Optics, Lawrence Berkeley National Laboratory, 1 Cyclotron Road, 94720 Berkeley, California, USA

Abstract

Dynamic switching of the vortex circulation in magnetic nanodisks by fast rising magnetic field pulse requires annihilation of the vortex core at the disk boundary during the first half-period of the high amplitude gyrotropic precession and reforming a new vortex with required sense of circulation. We study the influence of pulse parameters on the dynamics and efficiency of the dynamic vortex core annihilation in Permalloy nanodisks. We use magnetic transmission X-ray microscopy to experimentally determine the pulse rise time – pulse amplitude phase diagram for vortex circulation switching and show time-resolved evolution of magnetization in different regions of the phase diagram. The experimental phase diagram is compared with an analytical model based on Thiele's equation describing high amplitude vortex core motion in parabolic potential. We found that the analytical model is in a good agreement with experimental data for wide range of disk geometries. From the outputs of the analytical model and in accordance with our experimental finding we determine the geometrical restriction for dynamic vortex core annihilation and pulse parameters needed for the most efficient and fastest circulation switching. The comparison of our experimental results with micromagnetic simulations show that the micromagnetic simulations of 'ideal' disks with diameters larger than ~250 nm overestimate nonlinearities in susceptibility and eigenfrequency. This overestimation leads to a premature core polarity switching near the disk boundary, which then (in disagreement with experimental findings) prevents the core annihilation and circulation switching. We modified the micromagnetic simulation by introducing the 'boundary region' of reduced magnetization to fit the experimentally determined susceptibility and in these modified micromagnetic simulations we were able to reproduce experimentally observed dynamic vortex core annihilation and circulation switching.

I. INTRODUCTION

Magnetic vortices are curling magnetization structures formed in micro- and nanosized magnetic disks and polygons. They are known for having four different magnetization configurations (vortex states) that can be used for a multibit memory cell. The vortex states are defined by the polarity of the vortex core, pointing either up ($p = +1$) or down ($p = -1$) and by the circulation of the magnetization in the plane of the disk, curling either counterclockwise ($c = +1$), or clockwise ($c = -1$). They can be controlled by applying a static out-of-plane (polarity control [1]) or in-plane (circulation control [2]) magnetic fields, although the amplitude of these fields can be quite large. However, both the polarity and the circulation can be switched more effectively by using fast rising magnetic fields [3,4].

Selective switching of the circulation requires expelling the vortex core out of the disk and then reforming a new vortex with a required sense of spin circulation. We have recently demonstrated [4], that this can be achieved by using a fast rising in-plane magnetic field pulse that drives the vortex core into far-from-equilibrium gyrotropic precession and annihilates the vortex during the first half-period of

the precessional motion at the disk boundary. The resulting circulation of a new vortex is controlled by a disk asymmetry in the form of a thickness gradient and by the direction of the magnetic field pulse. This approach allows for a fast switching with the field amplitudes reduced by more than 50% when compared to the switching using static fields.

The dynamics of a magnetic vortex confined in soft ferromagnetic nanodisks excited resonantly by an in-plane alternating magnetic field or by a fast rising magnetic field pulse can be described as a forced harmonic oscillator using Thiele's equation of motion [5,6]. Its properties depend on the profile of the confining magnetostatic potential. The potential can be described either by parabolic terms [7], or more precisely including higher order terms in the energy expansion [8–10]. Micromagnetic simulations predict significant contribution of the higher order energy terms [8,9] leading to a nonlinear increase of the eigenfrequency as a function of the vortex core position. However, the experimental results obtained from eigenfrequency measurements at high amplitude rf field excitation or low amplitude rf field excitation in biasing field are often inconsistent with the simulations, showing a decrease of the eigenfrequency with an increasing amplitude[11] or a pinnig dominated eigenfrequency dependence [12,13]. Only recently, an experimental measurement of anharmonicity of a potential well in a FeV single crystal disk showed an ~10% increase of the eigenfrequency for vortex core displacements up to $0.4R$ [10].

In this paper, we present an experimental study of the process of dynamic annihilation of the magnetic vortices in micro- and nanosized magnetic disks. We investigate the range of disk diameters and thicknesses, in which the magnetic vortices can be dynamically annihilated, as well as the possible extension of this range by an appropriate selection of pulse rise time and amplitude. The experimental results are presented in section II. In section III we derive a simple, but well-fitting analytical model based on Thiele's equation of motion assuming a parabolic potential. In section IV we compare the experimental data and the analytical model with micromagnetic simulation. The discrepancy between the prediction of micromagnetic simulations and experimental data is discussed and a modified micromagnetic simulation, fitting to the experimental observation is presented.

II.   EXPERIMENTS

The dynamic annihilation of magnetic vortices was studied on a series of samples consisting from Permalloy ($Ni_{80}Fe_{20}$) disks with diameters ranging from 250 nm to 2500 nm and thicknesses from 20 nm to 50 nm. The disks were placed on gold coplanar waveguides which were used to generate in-plane magnetic field pulses up to 60 mT. To provide a circulation control, the disks were fabricated with a wedge-like thickness asymmetry using the shadowing effect of a 500-nm-thick polymethyl methacrylate (PMMA) mask and a directional ion beam sputtering of $Ni_{80}Fe_{20}$ with the sputtered particles incident at 15° from the film normal [4]. The entire structure was fabricated on a 200-nm-thick Si_3N_4 membrane to be able to conduct magnetic transmission x-ray microscopy (MTXM) [14] experiments.

Magnetic field pulses were generated by launching current pulses into the waveguide using a pulse generator (Agilent 81150A) allowing a precise setting of the rise time in the range of 2.5 – 8.0 ns and the amplitude of the pulses in the range of 1.0 – 50.0 mT. The pulse shapes were recorded on a 4-GHz oscilloscope (LeCroy WaveMaster 804Zi-A). Alternatively, for smaller disks where a faster rise time was needed, we used another pulse generator (Picosecond Pulse Labs 10,050A) with a fixed rise time of 250 ps.

The magnetization in the disks was imaged by XM-1, the full-field transmission soft x-ray microscope at beamline 6.1.2 at the Advanced Light Source (ALS) in Berkeley, CA. The images were captured for one circular polarization of the x-ray beam at the Fe L_3 edge (707 eV) with a spatial resolution of 25 nm

using x-ray magnetic circular dichroism (XMCD) as a source of magnetic contrast. The disks were imaged before, during and after application of the magnetic field pulses. The time-resolved experiments, where the snapshots of magnetization evolution in the disks were imaged at defined times during the magnetic pulse were based on a pump-probe technique enabling stroboscopic imaging of reproducible events [15]. The temporal resolution is given by the length of the photon flashes (70 ps), arriving at the sample at 3.05 MHz repetition frequency. The total acquisition time for each image is about 120 s, i.e. approx. 3.7×10^8 events are averaged per single image.

During the experiments, prior to the application of the magnetic field pulses we set the spin circulation in a disk into one state (e.g. clockwise) by applying an external static magnetic field in a defined direction. This was possible by exploiting the asymmetry in the disk thickness [4]. The pulsed magnetic field was then applied in the opposite direction and in case of the successful annihilation of a vortex the spin circulation in the disk switched (i.e. from clockwise to counterclockwise). In case of unsuccessful annihilation, the circulation stayed the same. This approach allowed for construction of a *pulse rise time – pulse amplitude* phase diagram of successful vortex annihilation (see Fig. 1). We are able to distinguish three distinct regions: (1) a region of low pulse amplitude and long rise time [Fig. 1(a), (b); red triangles], where the circulation switching was not detected, (2) a region of intermediate pulse amplitude and intermediate rise rime [Fig. 1(a), blue stars], where the circulation switching was detected and finally (3) a region of short rise time and high amplitude [Fig. 1(a), red dots], where again the circulation switching was not successful.

Time resolved experiments revealed the dynamics in each region. In region (1) the vortex core was not expelled out of the disk and gyrated freely in the disk with an unchanged polarity (see top inset in Fig. 1). In region (2) the pulse parameters were sufficient to expel the vortex core out of the disk. After an intermediate state where the disk was fully saturated [see left inset in Fig. 1(a)] a new vortex with a reversed circulation and a random polarity is formed [4]. The symmetric magnetic contrast apparent in these images corresponds to two vortex core trajectories for two opposite polarities of the vortex core [16], which were averaged together during a multitude of cycles of the pump-probe technique. The dynamics in region (3) shows the same symmetric contrast revealing core polarity switching, however here the disk did not reach a full saturation and the circulation did not reverse. This shows that the core polarity switching prevented annihilation and consequent circulation reversal, even when a stronger pulse than in region (2) was applied. The described behavior was consistent over all disk geometries. The character and boundaries of the normalized diagram stayed the same for disks with the same thickness, even when the radius was changed. With increasing disk thickness increased the region (2) moved towards top-right of the normalized phase diagram [Fig. 1 (b)]. In section III we present an analytical model describing underlying processes in the phase diagram.
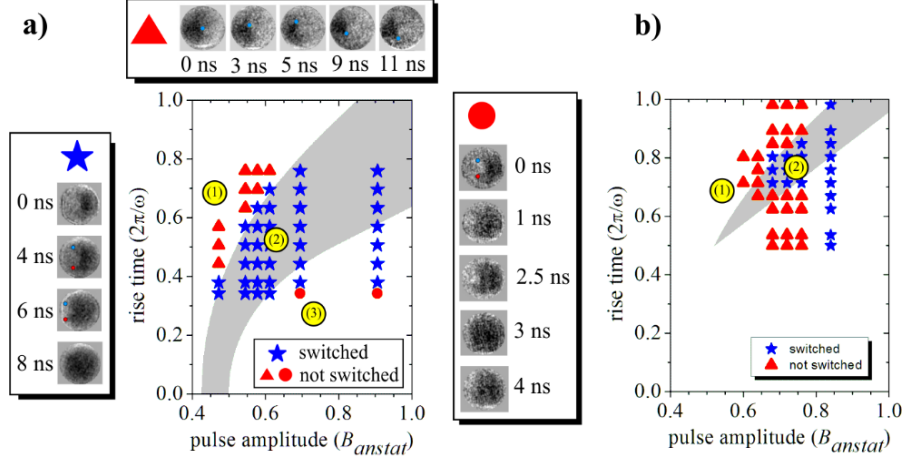
FIG1. (a) Pulse rise time – pulse amplitude phase diagram experimentally determined for a 1600-nm-wide, 20-nm-thick Permalloy disk. Estimated eigenperiod $2\pi/\omega$ = 7.9 ns, experimentally determined static annihilation field B_{anstat} = 19 mT. Red triangles [region (1)] represent a case of unsuccessful switching due to a low amplitude and/or long rise time of the magnetic pulse. Temporal evolution of the magnetization captured by a series of time-resolved MTXM images is depicted in the top inset. Blue stars [region (2)] represent a case, where successful core annihilation led to a circulation switching. Left inset shows temporal evolution of the magnetization in this region, showing full saturation at 8 ns which is followed by nucleation of a vortex with reversed circulation after X ns. Red dots [region (3)] represent a case, where the circulation switching was not achieved in spite of using the same rise time and larger pulse amplitudes than in region 2. Here, the maximum displacement of the vortex core was reached at 3 ns and at 4 ns the vortex core(s) already returned towards the disk center, indicating a continuous motion of the core without vortex annihilation and re-nucleation. Symmetric contrast in the MTXM images in the right and left insets is a combination of two symmetric core trajectories and thus indicates the core polarity reversal (either at vortex nucleation after its annihilation or directly during the core motion). (b) Phase diagram for a 1600-nm-wide, 30-nm-thick Permalloy disk. The region (2) moved towards top-right of the normalized phase diagram. The grey areas in the phase diagrams defines boundary of region (2) predicted by the analytical model (see section III).

III. ANALYTICAL MODELING

A vortex core trajectory in a magnetic disk during dynamic annihilation can be described by a simple analytical model based on Thiele's equation of motion [5,17]. When using a fast rising magnetic pulse with a rise time shorter or equal to the period of the vortex eigen-oscillation, the vortex core C gyrates about a point S, following circular trajectory [18]. The distance of the gyration center from the disk center is $s = R\chi B/(\mu_0 M_s)$, where χ is the static susceptibility of the vortex, B is the applied magnetic field and M_s is the spontaneous magnetization of the disk material [19]. As the coordinates of the gyration center depend on the magnitude of the magnetic field B, during the rise time of the magnetic pulse the point S is moving perpendicularly to the direction of the magnetic field with a velocity $v_s = R\chi B_{max}/(\mu_0 M_s t_{rise})$, where B_{max} is the maximum amplitude of the pulse and t_{rise} is the rise time of the pulse. Hence, the resulting trajectory of the vortex core is cycloidal with coordinates [20]: $x(t) = v_s[t - (1/\omega)\sin\omega t]$, $y(t) = (v_s/\omega)(1 - \cos\omega t)$, where ω is the eigenfrequency of the gyrotropic mode [17]. When the maximum amplitude of the pulse B_{max} is reached at $t = t_{rise}$, the vortex core trajectory changes to circular with a gyration center (static equilibrium point) at a distance $s_{max} = R\chi B_{max}/(\mu_0 M_s)$ from the disk center [see Fig. 1(a)]. The maximum amplitude of the vortex translational motion $C_{max} = s_{max} + \sqrt{[s_{max} - x(t_{rise})]^2 + y(t_{rise})^2}$ needs to fulfil the geometrical condition for the successful vortex annihilation: $C_{max}(B_{max}, t_{rise}) \geq R_{an}$. The vortex core is annihilated, when its distance from the disk center reaches the annihilation radius R_{an}, which is smaller than R due to the finite size of the vortex core. The value $R_{an} \sim 0.85R$ was estimated from experimental data – fitting upper boundary of the phase diagram (see Fig. 1) and confirmed by micromagnetic simulations [see Fig. 5(c)]. Another condition to be considered is associated with the vortex core velocity. If the core velocity exceeds the critical velocity the core polarity is switched [21] and the sense of the vortex core gyration is reversed [16]. The polarity reversal causes an offset of the initial core

position before it continues gyrating about the point S and as a result, the maximum amplitude of the vortex core translational motion is reduced. Although the vortex core may still reach the annihilation radius after polarity switching, it is at the cost of largely increased pulse amplitude and duration and this case is not considered in the model (pulses with an amplitude approaching or exceeding B_{anstat} and a sufficient duration will annihilate the vortex no matter what the exact dynamic behavior is).

For efficient dynamic switching (i.e. without core polarity reversal), the following condition for the maximum vortex core velocity v_{cmax} must be satisfied: $v_{cmax}(B_{max}, t_{rise}) < v_{crit}$, where $v_{cmax} = (2s_{max}/t_{rise})\sin(\omega t_{rise}/2)$ for $t_{rise} < \pi/\omega$ and $v_{cmax} = (2s_{max}/t_{rise})$ for $t_{rise} > \pi/\omega$ [20].
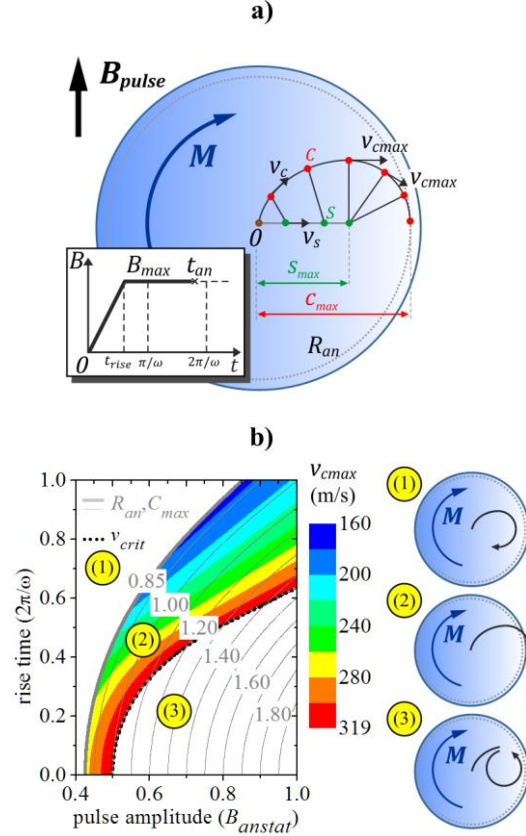
FIG. 2. (a) Sketch of the trajectory of the vortex core during a magnetic field pulse with a rise time. During the rise time of the magnetic pulse the gyration center S is moving perpendicularly to the direction of the magnetic field with a velocity v_s. The trajectory of the vortex core is cycloidal. At the maximum amplitude of the pulse B_{max} the vortex core trajectory changes to circular with a gyration center at a distance s_{max}. The vortex core is annihilated, when its maximum amplitude of the vortex translational motion C_{max} reaches the annihilation radius R_{an}. (b) Rise time – pulse amplitude phase diagram showing the region of successful vortex core annihilation [color-coded, marked (2)]. The region is defined by the two boundaries; annihilation radius R_{an} (thick gray line at $C_{max} = 0.85$) and critical velocity v_{crit} (black dotted line at $v_{cmax} = 320$ m/s). For the rise time – pulse amplitude combinations in the region [marked (1)] above annihilation radius boundary, the maximum amplitude of the translation motion of the vortex core is too low and the core gyrates inside the disk. For the rise time – pulse amplitude combinations in the region (3) below the critical velocity boundary the core switches its polarity and reverses its sense of gyration. The phase diagram is calculated for 20-nm-thick Permalloy disks with following material parameters: $M_s = 6.9 \times 10^5$ A/m, $\gamma = 2.9 \times 10^{11}$ rad·Hz/T, $v_{crit} = 320$ m/s. The rise time is normalized by the period of eigen-oscillation $2\pi/\omega$, the pulse amplitude is normalized by the static annihilation field B_{anstat} and maximum amplitude of the eigen-oscillation C_{max} (gray contour) is normalized by the disk radius R.

These conditions set a limit on the amplitude and rise time of the magnetic pulse needed for successful and efficient vortex core annihilation and form boundaries in a phase diagram displaying the region of successful switching [color-coded area in Fig. 1(b)]. The region is marked by two boundaries; first boundary results from the condition that the vortex core must reach the annihilation radius [thick gray line in Fig. 1(b)] and the second boundary is the result of the condition for the critical velocity [black dotted line in Fig. 1(b)].

Input parameters for the model are the rise time t_{rise}, the pulse amplitude B_{max}, the disk radius R, thickness L, it's susceptibility χ and eigenfrequency ω. The pulse parameters t_{rise} and B_{max} are used for construction of a phase diagram displaying the region of successful vortex annihilation [Fig. 1(a)] for disks with a given geometry. The last two parameters in the model (χ and ω) can be either determined experimentally or calculated from the material parameters of the modeled disk. It has been shown, that the susceptibility can be predicted with a reasonable precision by the rigid-core model [19] and the eigenfrequency by the pole-free model [17].

The eigenfrequency dependence on the disk geometry is approximately $\omega \sim L/R$, thus the vortex core velocity during gyration is proportional to the disk thickness L only ($v_c = \omega s \sim L$, where $s \sim R$ is the distance between the moving vortex and the point S). We can also normalize the pulse rise time with by the period of the eigen-oscillation and pulse amplitude by the static annihilation field. As a result, the shape of the phase diagram is the same for all disk diameters and depends on the thickness only. The lowest amplitude boundary remains the same for all thicknesses in the normalized phase diagram [see Fig 3(a)]. The intersection of the lowest amplitude boundary with the pulse amplitude axis at zero rise time indicates the minimum pulse amplitude which is sufficient to annihilate the vortex [~0.43 of the static annihilation field for our Permalloy disks, see Figs. 3(a), (b)]. The boundary for the critical velocity is moving to the left with increasing thickness [see Fig. 3(a)] and at a certain threshold [~23 nm for our Permalloy disks, see Fig. 3(b)] it is no longer possible to annihilate the vortex with a pulse with a zero rise time. By increasing the rise time, it is still possible to dynamically annihilate the vortex in thicker disks at the cost of an increased pulse amplitude. Finally, for disks thicker than 36.9 nm the minimum pulse amplitude equals the static annihilation field B_{anstat} [Fig. 3(b)].
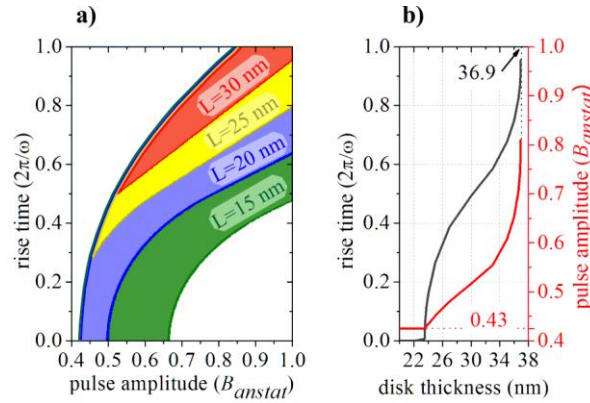
FIG. 3. (a) Phase diagram showing the regions of successful vortex core annihilation in Permalloy disks with different thicknesses. The lowest amplitude boundary on the left remains the same for all thicknesses. The critical velocity boundary is moving to the left with increasing disk thickness, i.e. the region of successful core annihilation is progressively shrinking. (b) Thickness dependence of the minimum pulse amplitude (red line) and the corresponding minimum pulse rise time (black line) needed for successful vortex core annihilation. For the disks with a thickness of 23 nm or less, the minimum pulse amplitude is 0.43 B_{anstat}. For disks with thicknesses above 36.9 nm the model does not predict the possibility of dynamic annihilation of the core with a pulse amplitude lower than B_{anstat} [the thickness limit is calculated assuming the same material parameters as in Fig 2(b)].

The pulse parameters, the rise time t_{rise}, the pulse amplitude B_{max} and the minimum pulse duration t_{an} (i.e. the predicted time at which the core reaches the annihilation radius R_{an}) can be used to calculate the energy cost associated with the vortex annihilation (resp. the circulation switching). Mapping the energy cost for each point in the region (2) of the phase diagram allows to find the specific pulse parameters for which the vortex annihilation is most efficient. Since the exact pulse energy $E = \int_0^{t_{an}} RI^2 \mathrm{d}t$ (R is the electrical resistance of the waveguide and I is the electric current) depends on the resistance of the waveguide used to generate the magnetic field pulse, we calculate the reduced energy

ε from the magnetic field pulse: $\varepsilon = \int_0^{t_{an}} B^2 dt$ in arbitrary units only. Assuming a linear rise time, we get $\varepsilon = B_{max}^2(t_{an} - \frac{2}{3}t_{rise})$ for the case where $t_{an} > t_{rise}$ and $\varepsilon = \frac{1}{3}t_{rise}(B_{max}t_{an}/t_{rise})^2$, when $t_{an} < t_{rise}$, i.e. the core is annihilated before the (theoretical) maximum pulse amplitude is reached. In Fig. 2(a)-(c) are efficiency parameters plotted in the pulse rise time – pulse amplitude phase diagrams for the disks with thicknesses L of 15, 20 and 30 nanometers. Note that the reduced energy in the phase diagram is independent of the disk radius. Although the period of eigen-oscillation increases for wider disks, it is compensated by a decrease of the annihilation field. For disks with thicknesses below ~20 nm, the most effective switching occurs when the pulse amplitude is slightly above the minimum value ($B_{max} = 0.47\ B_{anstat}$) and the rise time is short, but nonzero [$t_{rise} = 0.17\ (2\pi/\omega)$]. The region is marked by hashes in Figs. 2(a)-(b). For thicker disks, where the phase diagram becomes restricted by the critical core velocity and successful vortex annihilation cannot be achieved with short rise times. Then, the region of the most effective switching is located along the bottom-right boundary of the phase diagram and starts already at the minimum pulse amplitude [Fig. 4(c)].

The minimum pulse duration [Figs. 4(d)-(e)] does not exactly correspond to the region of the least energy cost; unlike the reduced energy, the minimum pulse duration depends the radius of the disk. The regions of fastest switching for thinner disks [Figs. 4(d)-(e), marked by hashes] are located around the minimum rise time and maximum pulse amplitude. For thick disks the region of fastest switching is located along the right boundary of the phase diagram [Fig. 4(f)]. By comparing the absolute values of ε in Figs. 4(a)-(c) and t_{an} in Figs. 4(d)-(f), we can see that the switching becomes more effective with decreasing disk thickness and also the time to annihilation can be shortest in thinnest disks. However, for thinner disks the position of the region of the fastest switching does not correspond with the region of minimum ε [compare Fig. 4(d) and Fig 4(a), respectively] and the choice between fast or effective switching must be made.
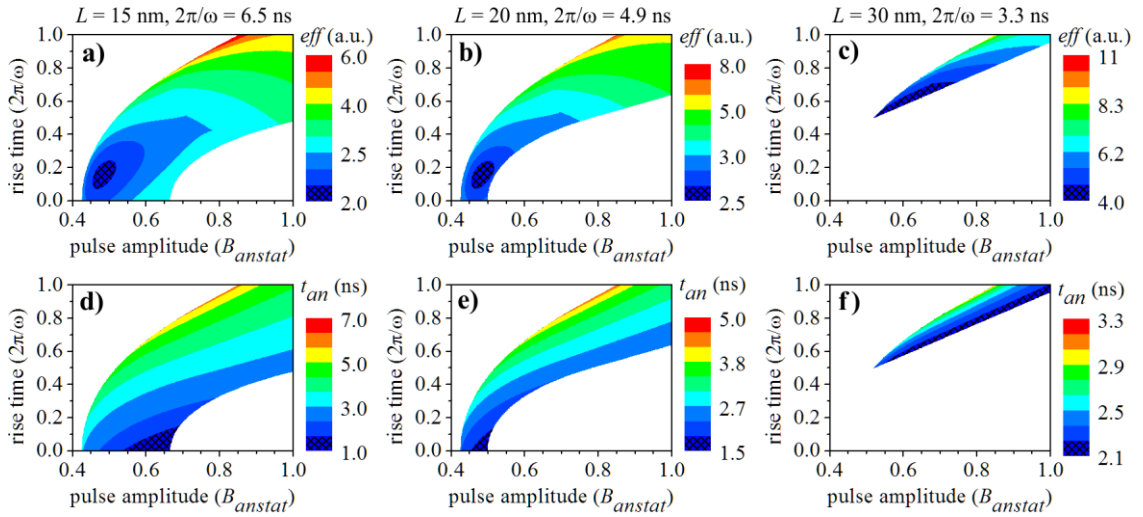
FIG. 4. Pulse rise time – pulse amplitude phase diagrams showing the reduced energy ε needed for the vortex circulation switching (a)-(c) and shortest annihilation times t_{an} (d)-(e). The regions of the most efficient switching (least energy cost) and shortest annihilation times are marked by hashes. The phase diagrams were calculated for Permalloy disks with a radius R=500 nm and thicknesses L = 15, 20 and 30 nm. Material parameters used for calculation of the phase diagrams were the same as in Fig. 2.

IV. MICROMAGNETIC SIMULATIONS

The predictions of the analytical model agreed with micromagnetic simulations in OOMMF [22,23] the simulations agreed with the predictions of the analytical model for disks with radius R up to ~125 nm. For larger disks of all thicknesses, the vortex core velocity exceeded the critical velocity within few picoseconds after the beginning of the pulse which lead to core polarity switching. The micromagnetic simulation predicts large nonlinearity in displacement susceptibility $\chi_d = dS/dB$ [Fig. 3(a); orange line with circles]. Due to this nonlinearity, at the beginning of the pulse where the displacement susceptibility is higher, the gyration center in micromagnetic simulation is located further than linear model predicts. For instance, a pulse amplitude $B = 0.5B_{anstat}$ corresponds to a gyration center S at $0.5R$ according to linear model [Fig. 5(a) grey line], whereas according to micromagnetic simulation the position of S is at $0.85R$ [Fig. 5(a) orange line with circles]. This increase in the gyration radius leads to an increase of the core velocity above the critical velocity. We can overcome the unwanted polarity switching at the beginning of the pulse by using a pulse with a nonzero rise time. However when the core approaches the disk boundary, its velocity again exceeds the critical velocity, which leads to polarity reversal and a consequent change in the sense of gyration [see Fig. 5(b)]. This reversal at the disk boundary, which is always present in simulation of disks with radii larger than ~ 500 nm is caused by anharmonicity in the potential energy well of the vortex leading to a nonlinear, vortex-core-position-dependent eigenfrequency [8,9,24,25]. From displacement susceptibility $\chi_d(S)$, we can obtain the local eigenfrequency $\omega(S) = \frac{1}{2}\gamma M_s \frac{\xi^2}{\chi_d(S)}$, here we assume $\xi = 2/3$ (pole-free model magnetization distribution [17]). Note, that this approach is more suited to the calculation of eigenfrequency of small amplitude vortex core gyration about gyration center position S shifted from the disk center by static biasing field. In our case of the large gyration amplitude, the eigenfrequency in the position of the vortex core C may be lower [24]. The local eigenfrequency $\omega(S)$ rapidly increases for the core displacements larger than $0.6R$ [see Fig. 5(d) orange line with circles]. The increase in eigenfrequency drives the core velocity above the critical value and the core polarity close to the disk boundary switches [Fig. 5(b)].

This result of micromagnetic simulation is in contradiction to our experimental observation, where we were able to annihilate the vortex core in the disks with radii up to 1.25 μm. The resolution of XM-1 microscope allowed us to directly measure a shift of the vortex core in an applied magnetic field with sub-100-nm precision. Comparison of the experimentally measured displacement susceptibility for 1600-nm-wide, 20-nm-thick disk [Fig. 5(a); blue line with squares] with micromagnetic simulation [Fig. 5(a); orange line with circles] reveals the overestimation of the nonlinearity in displacement susceptibility by the micromagnetic simulation.

We were able to reproduce the experimental displacement susceptibility curve in micromagnetic simulations [see Fig. 3(a)], blue line with squares and green line with triangles, respectively) by gradual decrease of the spontaneous magnetization of the disk material near the edge [from 690 kAm[-1] to 310 kAm[-1] in the 80-nm-wide 'boundary zone', see insets in Figs. 5(b) and 5(c)]. After this modification, it is possible to annihilate the vortex also in micromagnetic simulation [see Fig. 3(c)]. The eigenfrequency calculated from corrected simulation and from experimentally measured displacement susceptibility stays close to the eigenfrequency used in the linear model [see Fig. 5(d)] and the vortex core can reach the annihilation radius without exceeding the critical velocity.
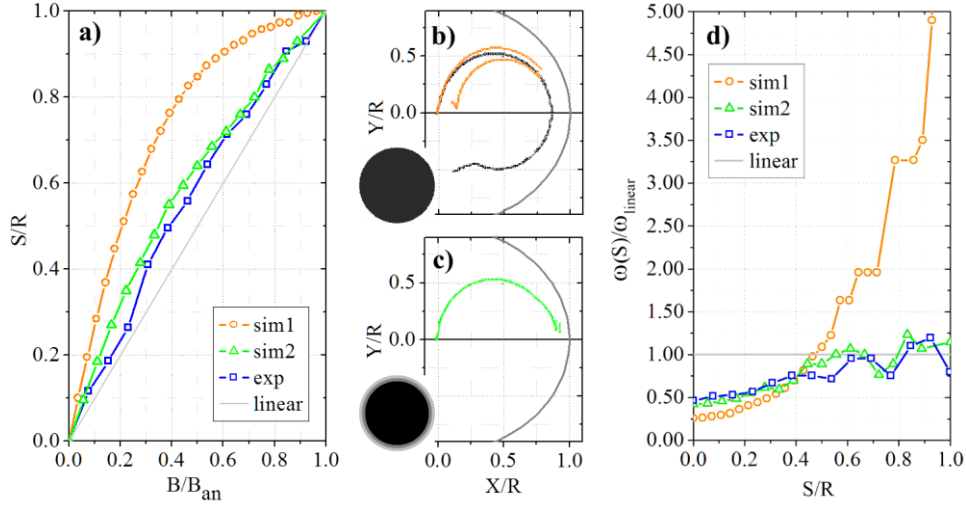
FIG. 5. (a) comparison of simulated displacement susceptibility of the 1600 nm wide, 20 nm thick disk with uniform M_s (sim1 – red line with circles), simulated displacement susceptibility of the same disk, where the spontaneous magnetization of the disk material was gradually decreased from 690 kAm^{-1} to 310 kAm^{-1} in the 80-nm-wide region around the disk perimeter (sim2 – green line with triangles) and the displacement susceptibility determined directly from the experimental measurements of the shift of the vortex core in an increasing applied magnetic field by MTXM (exp – blue line with squares). Linear susceptibility, used in analytical models is plotted as a gray line. (b) simulated vortex core trajectories in the disk with uniform magnetization (nonlinear susceptibility). A magnetic field pulse of 10 mT is not enough to reach the annihilation radius (black trajectory). A slight increase of the magnetic field amplitude to 11 mT drives the vortex core into the nonlinear region, where the eigenfrequency of the translational motion and thus also the vortex core velocity are increased, which leads to unwanted polarity switching. Switched core then continues with inverted sense of gyration towards the disk center (red trajectory). (c) simulated vortex core trajectory in the disk with magnetization decreasing towards the edge (linearized susceptibility). A magnetic pulse of 9 mT is sufficient to drive the vortex core into the annihilation region and the vortex is successfully annihilated (green trajectory).

The linear behavior of the displacement susceptibility in real disks may be caused by shape imperfections, lateral roughness and due to other deteriorations of the magnetic properties of the disk material close to the disk edge, e.g. by oxidation. It cannot be explained by the lateral roughness only, because the lateral roughness at the edges of our disks was approx. 20 nm (estimated from SEM images), whereas the width of the boundary region necessary for reproducing the experimental data is 4x larger. We observed an additional increase of the nonlinearity in displacement susceptibility for larger disks, however the experimentally determined nonlinearity in displacement susceptibility was still significantly smaller than the predictions of micromagnetic simulations (2.5-µm-wide disks, data not shown). Similar, weaker than expected nonlinearity in displacement susceptibility was reported for 3-µm-wide Permalloy disks measured by Lorentz transmission electron microscopy by Uhlig et al. [26]. The existence of higher-order term (beyond parabolic approximation) in the potential energy well resulting in a parabolic dependence of $\omega(S)/\omega_0$ and 10% increase ~0.3R was recently reported in FeV single crystal disks [10]. In our case, a similar dependence in experimentally determined eigenfrequency can be seen for static core displacements up to 0.4R [Fig. 5(d)], beyond this point the experimental data do not follow a clear trend (i.e. parabolic dependence) and stay in the vicinity of ω_{linear}. This comparison shows that for large amplitude vortex core gyrations the assumption of linear susceptibility provides a good approximation and that the micromagnetic simulations of 'ideal' disks grossly overestimate the nonlinearity in displacement susceptibility (anharmonicity of the vortex potential well) for large core displacements.

CONCLUSION

In summary, we have studied the influence of the pulse parameters on the dynamics and efficiency of the vortex core annihilation in Permalloy nanodisks. The experimentally determined pulse risetime – pulse amplitude phase diagram was successfully reproduced with an analytical model based on Thiele's equation describing vortex core motion in a parabolic potential. We found that the analytical model is in a good agreement with experimental data for a wide range of disk geometries. From both the analytical model the experimental findings we have determined the geometrical condition for dynamic vortex core annihilation and the pulse parameters giving the most efficient and fastest circulation switching.

However, micromagnetic simulations of the vortex core annihilation in 'ideal' disks did not reproduce the experimental behavior. This is due to the fact that the nonlinearities in displacement susceptibility and eigenfrequency of 'ideal' disks with diameters larger than ~250 nm are overestimated with respect to the experimentally determined values. This overestimation leads to a premature core polarity switching near the disk boundary which prevents the core annihilation and subsequent circulation switching. We modified the micromagnetic simulation by introducing a 'boundary region' of reduced magnetization to simulate the experimentally determined displacement susceptibility. This results in linearization of the displacement susceptibility and the modified micromagnetic simulation shows a good agreement of the dynamic vortex core annihilation with the experimental observations. Assumption of a non-parabolic potential with higher order energy terms, which may be more precise for the description of vortex core motion within 0.4 R from the disk center [10], does not make a significant correction to the parameters inferred from the linear susceptibility model. We conclude that the linear susceptibility model (i.e. a parabolic potential) is appropriate for the description of large amplitude vortex core gyration in real disks.

References

[1]   N. Kikuchi, S. Okamoto, O. Kitakami, Y. Shimada, S. G. Kim, Y. Otani, and K. Fukamichi, J. Appl. Phys. **90**, 6548 (2001).

[2]   M. Schneider, H. Hoffmann, and J. Zweck, Appl. Phys. Lett. **79**, 3113 (2001).

[3]   B. Van Waeyenberge, a Puzic, H. Stoll, K. W. Chou, T. Tyliszczak, R. Hertel, M. Fähnle, H. Brückl, K. Rott, G. Reiss, I. Neudecker, D. Weiss, C. H. Back, and G. Schütz, Nature **444**, 461 (2006).

[4]   V. Uhlíř, M. Urbánek, L. Hladík, J. Spousta, M.-Y. Im, P. Fischer, N. Eibagi, J. J. Kan, E. E. Fullerton, and T. Sikola, Nat. Nanotechnol. **8**, 341 (2013).

[5]   A. A. Thiele, Phys. Rev. Lett. **30**, 230 (1973).

[6]   D. L. Huber, Phys. Rev. B **26**, 3758 (1982).

[7]   V. Novosad, F. Fradin, P. Roy, K. Buchanan, K. Guslienko, and S. Bader, Phys. Rev. B **72**, 024455 (2005).

[8]   K.-S. Lee and S.-K. Kim, Appl. Phys. Lett. **91**, 132511 (2007).

[9]   K. Y. Guslienko, R. H. Heredero, and O. Chubykalo-Fesenko, Phys. Rev. B **82**, 014402 (2010).

[10]   O. Sukhostavets, B. Pigeau, S. Sangiao, G. de Loubens, V. Naletov, O. Klein, K. Mitsuzuka, S. Andrieu, F. Montaigne, and K. Guslienko, Phys. Rev. Lett. **111**, 247601 (2013).

[11]   B. Pigeau, G. de Loubens, O. Klein, A. Riegler, F. Lochner, G. Schmidt, and L. W. Molenkamp, Nat. Phys. **7**, 26 (2011).

[12]   R. L. Compton, T. Y. Chen, and P. A. Crowell, Phys. Rev. B **81**, 144412 (2010).

[13]   T. Y. Chen, M. J. Erickson, P. A. Crowell, and C. Leighton, Phys. Rev. Lett. **109**, 097202 (2012).

[14]   P. Fischer, Mater. Today **13**, 14 (2010).

[15] S. Kasai, P. Fischer, M.-Y. Im, K. Yamada, Y. Nakatani, K. Kobayashi, H. Kohno, and T. Ono, Phys. Rev. Lett. **101**, 237203 (2008).

[16] S.-B. Choe, Y. Acremann, A. Scholl, A. Bauer, A. Doran, J. Stöhr, and H. A. Padmore, Science **304**, 420 (2004).

[17] K. Y. Guslienko, B. A. Ivanov, V. Novosad, Y. Otani, H. Shima, and K. Fukamichi, J. Appl. Phys. **91**, 8037 (2002).

[18] In the model we always consider only one period of the eigen-oscillation (or less) thus we can neglect the damping term in the Thiele's equation and assume a circular trajectory.

[19] K. Guslienko, V. Novosad, and Y. Otani, Appl. Phys. Lett. **78**, 3848 (2001).

[20] See supplementary material for detailed description of the presented model.

[21] K. Guslienko, K.-S. Lee, and S.-K. Kim, Phys. Rev. Lett. **100**, 027203 (2008).

[22] M. J. Donahue and D. G. Porter, Natl. Inst. Stand. Technol. Gaithersburg, MD (1999).

[23] The spontaneous magnetization M_s, gyromagnetic ratio γ and damping parameter A were determined experimentally using ferromagnetic resonance on blanket film samples, with values: $M_s = 690$ kA/m, $\gamma = 2.09 \times 10^{11}$ rad Hz/T and A = 0.0072.

[24] K. S. Buchanan, P. E. Roy, F. Y. Fradin, K. Y. Guslienko, M. Grimsditch, S. D. Bader, and V. Novosad, J. Appl. Phys. **99**, 08C707 (2006).

[25] X. Cheng, K. Buchanan, and R. Divan, Phys. Rev. B **79**, 172411 (2009).

[26] T. Uhlig, M. Rahm, C. Dietrich, R. Höllinger, M. Heumann, D. Weiss, and J. Zweck, Phys. Rev. Lett. **95**, 237205 (2005).